Rapid Communications

Anomalous wave statistics induced by abrupt depth change

C. Tyler Bolles,[1,2] Kevin Speer,[1,3] and M. N. J. Moore[1,4]

[1]*Geophysical Fluid Dynamics Institute, Florida State University, Tallahassee, Florida 32306, USA*

[2]*Department of Mathematics, University of Michigan, Ann Arbor, Michigan 48109, USA*

[3]*Earth, Ocean and Atmospheric Sciences, Florida State University, Tallahassee, Florida 32304, USA*

[4]*Department of Mathematics, Florida State University, Tallahassee, Florida 32304, USA*

(Received 20 September 2018; published 22 January 2019)

Laboratory experiments reveal that variations in bottom topography can qualitatively alter the distribution of randomized surface waves. A normally distributed, unidirectional wave field becomes highly skewed and non-Gaussian upon encountering an abrupt depth change. A short distance downstream, wave statistics conform closely to a gamma distribution, affording simple estimates for skewness, kurtosis, and other statistical properties. Importantly, the exponential decay of the gamma distribution is much slower than Gaussian, signifying that extreme events occur more frequently. Under the conditions considered here, the probability of a rogue wave can increase by a factor of 50 or more. We also report on the spectral content of the waves produced in the experiments.

DOI: 10.1103/PhysRevFluids.4.011801

Although once regarded as mythical, rogue waves have now been recorded in oceans across the globe and are no longer doubted as a real phenomenon [1–6]. The existence of these abnormally large waves is fundamentally tied to non-normal statistics; if governed by Gaussian statistics, their occurrence would be exceedingly rare and the danger posed modest. From this perspective of anomalous behavior, rogue waves can be considered under the more general framework of turbulent dynamical systems [7–13]. Several physical mechanisms have been demonstrated to produce rogue waves, most notably the Benjamin-Feir (BF) instability that occurs in deep water [1,14–21] as well as in optical systems [22]. Other proposed mechanisms include wind excitation [23–25], opposing currents [19,26,27], and geometric ray focusing from two-dimensional (2D) bathymetry [28,29].

A few recent studies have suggested that anomalous behavior can arise in the much simpler setting of a *unidirectional* wave field propagating over a *one-dimensional* variable bottom [30–36]. Since these studies are performed outside of the deep-water regime, the BF instability is absent, as are the other mechanisms listed above [no wind or current and bathymetry is strictly one-dimensional (1D)]. Intriguingly, many of these studies identify certain locations at which the deviation from Gaussianity is maximized and, thus, rogue waves are most likely. Such locations are analogous to the "hot spots" observed in microwave systems [37], but without the benefit of 2D geometric focusing.

Inspired by this line of thought, we perform laboratory experiments to examine the statistics of unidirectional waves propagating over a 1D, variable bottom, in the shallow-to-moderate depth regime (outside the influence of the BF instability). Unlike previous experiments that featured gradual slopes of 1:20 [35], we focus on abrupt depth transitions. In particular, we consider waves propagating over a step in bottom topography—akin to the step potentials considered early on in quantum mechanics that helped lay the foundation for scattering theory. In accordance with previous results, we find the deviation from Gaussian behavior to be maximized at certain locations. Whereas previous studies only quantified non-Gaussianity in terms of a few statistical moments, we find the complete surface-displacement statistics in these anomalous regions to be accurately described by

 ©2019 American Physical Society

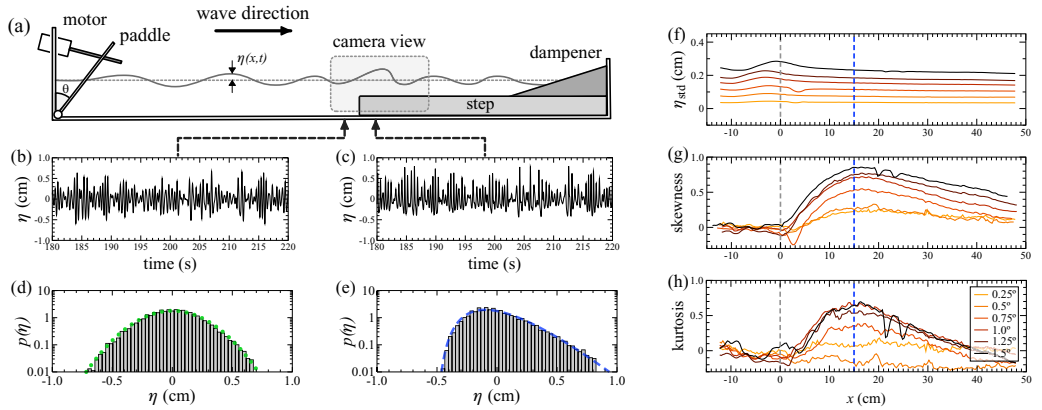

FIG. 1. (a) Experimental schematic. (b),(c) Surface displacement measured at a representative upstream and downstream location. (d),(e) Corresponding histograms. (f) η_{std} as it varies in space for six different driving amplitudes. (g),(h) Similar for skewness and kurtosis, showing an anomalous region at $x = 15$ cm where deviation from Gaussian is most pronounced.

a gamma distribution. This clean characterization offers a precise test for theories and may help differentiate the various rogue-wave producing mechanisms.

Experiments. As diagramed in Fig. 1(a), our experiments consists of a long, narrow wave tank (6 m long $\times$ 20 cm wide $\times$ 30 cm high) with waves generated by a plexiglass paddle that is hinged to the bottom and driven by a five-phase stepper motor (0.72° precision). A horse-hair dampener located at the far end minimizes reflections back into the tank (measured reflections are less than 10% [38,39]). To create a depth transition, a plexiglass step (2 m long) is inserted at the far end. Spacers allow us to vary the height of the step and thus the ratio of the two depths. Reflections due to the step itself can be estimated from linear scattering theory, giving reflection coefficients of less than 20% for the conditions considered here [38].

Our primary technique for measuring waves is optical, with video images taken by a Nikon D3300 from the sideview at 60 fps. The free surface is illuminated by light-emitting diode lights that run along the bottom of the tank and provide the contrast necessary to extract surface displacements from images with submillimeter resolution [40]. The camera is focused on a 60 $\times$ 34 cm window surrounding the depth change, which was determined to be the region of greatest statistical interest. As complementary measurements, we deploy two AWP-24 depth gauges, which enable higher temporal resolution (5 ms response time) at fixed locations. We use these gauges primarily for corroboration, as the optical measurements provide the spatial information crucial for identifying anomalous regions.

Central to our study, we aim to create a *randomized* incoming wave field so that we can examine how its characteristics are modified by the depth change. We therefore specify the paddle angle, $\theta(t)$, with a pseudorandom signal that is precomputed to mimic a Gaussian random sea [2,36,41]:

$$\theta(t) = \theta_0 + \Delta\theta \sum_{n=1}^{N} a_n \cos(\omega_n t + \delta_n), \tag{1}$$

$$a_n = \sqrt{\frac{2\Delta\omega}{\pi^{1/2}\sigma_\omega}} \exp\left(-\frac{(\omega_n - \omega_0)^2}{2\sigma_\omega^2}\right). \tag{2}$$

Here, the angular frequencies are evenly spaced $\omega_n = n\Delta\omega$ with step size $\Delta\omega = (\omega_0 + 4\sigma_\omega)/N$, where ω_0 and σ_ω represent the mean and the bandwidth of ω, respectively. We set $\omega_0 = \sigma_\omega = 12.5$ rad/s, corresponding to a peak forcing frequency of 2 Hz and bandwidth of 2 Hz. Importantly,

TABLE I. Basic experimental parameters and scales.

Parameter	Upstream value	Downstream value
Peak forcing frequency	2 Hz	N/A
Depth, h	12.5 cm	3 cm
Peak wavelength, λ	38 cm	25 cm
Peak wave number, k	0.17 rad/cm	0.25 rad/cm
Dimensionless depth, kh	2.1	0.76
Wave steepness, $s \sim k\eta_{\mathrm{std}}$	$0.5\text{–}5 \times 10^{-2}$	$0.8\text{–}8 \times 10^{-2}$
Ursell number, Ur	N/A	0.03–0.3

the phases δ_n are uniformly distributed random variables. We fix $N = 3000$, which sets a fundamental period of $T = 300$ s.

The driving amplitude is determined by $\Delta\theta$, which we vary in the range 0.125°–2.0°. This range was selected to probe the various regimes of wave behavior: the low end produces linear waves, the middle produces weak to moderate nonlinear effects, and the high end generates strongly nonlinear waves that occasionally break. We have also varied the step height systematically and found results to be robust for depth ratios in the range 0.2–0.5 [38]. We therefore fix the step height in all results reported here, so that the effects of driving amplitude can be explored in detail. In these representative experiments, the upstream and downstream depths are 12.5 and 3 cm, respectively, creating a depth ratio of 0.24. Table I lists some important scales that result from our choices of depths and forcing parameters, in particular, the peak upstream and downstream wavelengths λ and wave numbers $k = 2\pi\lambda^{-1}$, as determined by the dispersion relation $\omega^2 = gk \tanh kh$.

Results. In the absence of depth variations, the randomized forcing from Eq. (1) produces *normally distributed* surface waves, as is consistent with linear wave theory. With a depth transition, however, we find that wave statistics can vary in space and deviate strongly from Gaussian. Figures 1(b) and 1(c) show measurements of the surface displacement $\eta(t)$ taken at a representative upstream and downstream location. While both signals exhibit a random character, the upstream measurements fluctuate symmetrically about the mean, whereas the downstream signal shows events biased toward large, *positive* displacement. These observations are made more apparent by the corresponding histograms in Figs. 1(d) and 1(e). Indeed, the upstream measurements are distributed symmetrically about the mean and, in fact, follow a Gaussian distribution closely (green dotted curve). The downstream measurements, however, deviate from Gaussian and skew heavily toward positive displacement.

These results indicate very different behaviors on either side of the depth change, but offer no detail on how wave properties vary in space. Fortunately, the optical measurements allow us to extract statistics continuously in space—a capability crucial for identifying potentially highly localized regions of anomalous behavior [36]. First, to estimate the scale of wave amplitudes involved, Fig. 1(f) shows the standard deviation η_{std} as it varies in space for six different driving amplitudes $\Delta\theta$ (see legend). Here, x is the distance from the step, with $x < 0$ upstream and $x > 0$ downstream. First, we observe that η_{std} is nearly uniform in space for all driving amplitudes, suggesting that the depth change does not significantly alter the basic scale of wave amplitude. This finding is consistent with previous results [36]. Second, as evident by the even spacing between curves, η_{std} grows linearly with the driving amplitude (we find $\eta_{\mathrm{std}} \approx 0.15\Delta\theta$). The range of observed η_{std}: 0.03–0.3 cm, combined with the values in Table I, permits estimates for the characteristic wave steepness, $s \sim k\eta_{\mathrm{std}}$, which roughly indicates the strength of nonlinearity present. In Table I, we show the steepness ranges upstream of and downstream from the depth transition, along with the downstream Ursell number $\mathrm{Ur} = 3k\eta_{\mathrm{std}}/(2k^3h^3)$ [42], which provides a more precise measure of nonlinearity in shallow water.

Next, to determine where and how wave statistics deviate from Gaussian we inspect some higher-order moments. Figures 1(g) and 1(h) show the skewness and (excess) kurtosis as they

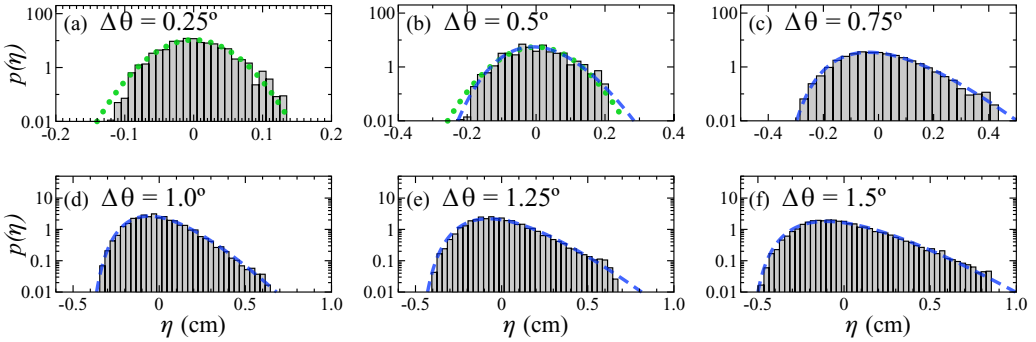

FIG. 2. Histograms of η sampled at the anomalous location ($x = 15$ cm) for six different driving amplitudes, $\Delta\theta$. For $\Delta\theta > 0.5^\circ$, behavior is non-Gaussian and the gamma distribution (blue dashed curve) provides a robust statistical description.

vary in space for the same set of driving amplitudes. Since both are zero for a normal distribution, these quantities indicate how wave statistics deviate from Gaussian. Compared to η_{std}, these higher moments exhibit more complex dependence on position and driving amplitude. For small driving amplitudes, skewness and kurtosis remain relatively small throughout the domain. For larger amplitudes, both grow substantially upon encountering the depth change and reach a maximum somewhere downstream. Remarkably, the location of the maximum, $x = 15$ cm, is the same for both skewness and kurtosis and for all driving amplitudes tested. This consistency indicates a small region of highly intensified wave activity, whose location is independent of driving amplitude.

We remark that the location and size of the anomalous region are on the scale of the characteristic wavelengths given in Table I. Farther downstream, skewness and kurtosis both decay to near zero, indicating a recovery of Gaussian statistics. Dissipative effects, such as contact-line dynamics, viscous layers, and wave breaking may be responsible for this relaxation to a Gaussian state.

The anomalous location, $x = 15$ cm, was in fact the position selected for the "representative" downstream measurements shown in Figs. 1(c) and 1(e). Closer inspection of the histogram (e) yields a few observations: (1) The measurements skew heavily toward positive displacement; (2) due to the log scale, the apparent linear decrease to the right indicates an exponential tail; (3) the decay is much more rapid on the left and is consistent with compact support on that side; and (4) the mean displacement always remains zero. Perhaps the simplest conceivable description that accounts for observations (1)–(4) is a mean-zero gamma distribution

$$p(\eta) = \frac{e^{-\alpha}}{\eta_\gamma \Gamma(\alpha)} \left(\alpha + \frac{\eta}{\eta_\gamma}\right)^{\alpha-1} \exp\left(-\eta/\eta_\gamma\right), \tag{3}$$

valid for $\eta \in [-\alpha\eta_\gamma, \infty)$. Here, η_γ and α are the scale and shape parameters, respectively, which were fit to obtain the blue dashed curve in Fig. 1(e). Remarkably, this fit accurately describes the measurements over two decades of statistics [$0.02 \leqslant p(\eta) \leqslant 2$]. Note that the relatively slow decay of Eq. (3) (compared to Gaussian) indicates an increased frequency of extreme events.

We now aim to test the robustness of this statistical description to changes in driving amplitude. Accordingly, Figs. 2(a)–2(f) show histograms of η, all taken at the anomalous location $x = 15$ cm, with the driving amplitude $\Delta\theta$ systematically increased. The first two, (a) and (b), deviate only slightly from Gaussian (green dotted curves), with the second showing hints of transitioning toward a skewed distribution. The next four, (c)–(f), all skew heavily toward positive η. Indeed, each of these histograms conforms closely to a gamma distribution (blue dashed curves), with η_γ and α fit for each. We therefore conclude that Eq. (3) robustly describes wave statistics within the anomalous region, once a threshold amplitude is exceeded ($\theta > 0.5^\circ$ or $\eta_{\text{std}} > 0.07$ cm).

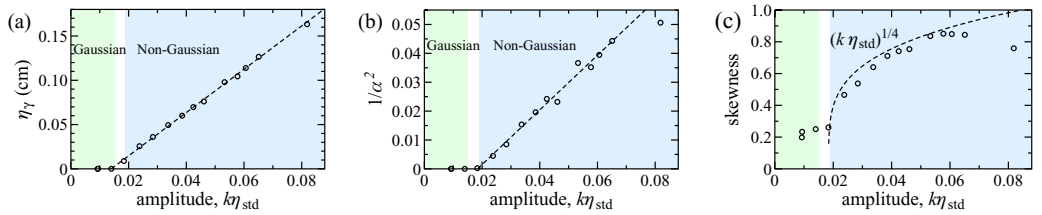

FIG. 3. (a),(b) Variation of the parameters η_γ and α with driving amplitude. Small amplitudes generate Gaussian statistics (green region), and larger amplitudes give rise to the gamma distribution (blue region), with η_γ and α estimated for each. Both η_γ and α^{-2} increase nearly linearly with amplitude. (c) The linear fit of α^{-2} leads to a power-law prediction for skewness, which compares well with direct measurements.

It is perhaps surprising that Eq. (3) appears to describe the *complete* distribution of measured wave statistics (over two decades) with only two free parameters. What physical meaning do these parameters carry? The first, η_γ, sets a length scale of the gamma distribution, and the second, $\alpha > 1$, controls its shape: large α signifies a nearly symmetric distribution and smaller α a highly skewed one. By analyzing how these parameters change with experimental conditions, we can understand the corresponding changes in anomalous wave activity. Accordingly, Figs. 3(a) and 3(b) show the values of these parameters extracted from 15 different experiments, in which the driving amplitude was systematically increased. To present these results in a broader context, we convert the driving amplitude, $\Delta\theta$, to downstream dimensionless wave amplitude (or characteristic steepness) $k\eta_{\rm std}$, where $k = 0.25$ rad/cm and $\eta_{\rm std}$ is taken directly from measurements. At small amplitudes, the statistics are nearly Gaussian as indicated by the green region in Figs. 3(a) and 3(b). For larger amplitudes, $k\eta_{\rm std} > 0.02$, the gamma-distribution fit becomes valid (blue region) and the two parameters η_γ and α can be extracted. In this regime, η_γ increases and α decreases with amplitude, meaning that, not only is the gamma distribution growing in length scale but it is also becoming increasingly skewed. More precisely, we have found that η_γ and α^{-2} grow nearly linearly with $k\eta_{\rm std}$ (dashed lines). The linear growth of η_γ has a simple interpretation, namely, the driving amplitude directly sets the length scale of the gamma distribution. We have no such rationalization for the linear growth of α^{-2}, however, and simply report it as an experimental finding.

The clean characterization of the near-complete surface-displacement statistics via only two parameters allows one to immediately predict any statistical feature of η, for example, its moments. In particular, Eq. (3) has a skewness of $2\alpha^{-1/2}$. The observed linear growth of α^{-2} therefore implies the scaling law: skewness $\sim (k\eta_{\rm std})^{1/4}$. In Fig. 3(c) we show, for each of the 15 experiments, the skewness taken directly from the measurements (circles), along with this prediction (dashed curve). The scaling law accounts for the experimental trend remarkably well. We note that in obtaining this prediction, the formula $2\alpha^{-1/2}$ was applied directly to the linear estimate of α^{-2}, with no additional fitting parameters introduced.

Lastly, we briefly report on the spectral content of the waves generated in our experiments, in particular how the spectrum is modified by the depth change. Figure 4 shows the power spectrum of the displacement, η, and slope, η_x, taken at the same representative upstream and downstream locations ($x = -10$ cm and $x = 15$ cm, respectively). The slope is extracted via numerical differentiation (with noise mitigation techniques applied). In the upstream measurements, the power spectra of both η and η_x peak near the dominant-forcing frequency of 2 Hz (faint vertical line), then decay rapidly to a noise level of about 10^{-5}. The downstream measurements also peak around 2 Hz, but decay more gradually at high frequencies. In particular, both spectra decay algebraically, with powers estimated as -5 for displacement and -4 for slope (red dashed lines). These relatively slow decay rates are broadly consistent with previous studies [36,43], and indicate that waves within the anomalous region possess an elevated level of high frequencies. Further, these measurements support the idea that non-Gaussian wave statistics are associated with

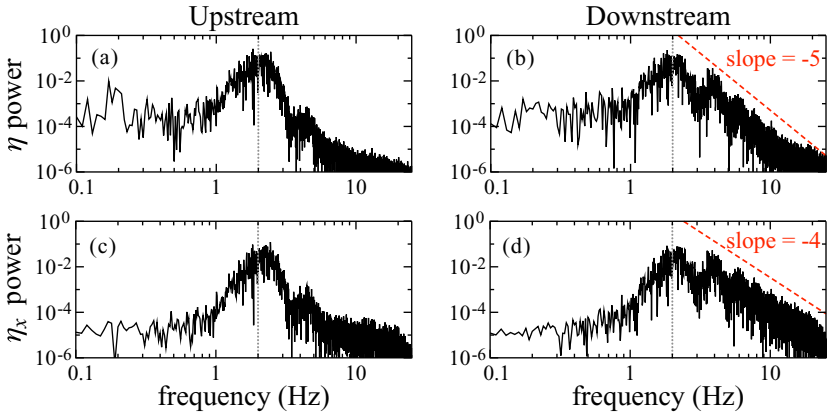

FIG. 4. Power spectra of displacement (top) and surface slope (bottom) taken at representative upstream and downstream locations, along with estimated power laws.

an out-of-equilibrium spectrum [31,34,36]. We also note the presence of higher harmonics (4, 6, and 8 Hz) in the downstream spectra, which are likely due to resonance with the upstream forcing.

Discussion. These experiments reveal some basic, quantitative information on the emergence of anomalous waves from abrupt changes in bottom topography. We find the deviation from Gaussian behavior to be maximized a short distance downstream from a depth change, at which point wave statistics conform closely to a gamma distribution. Once a critical depth ratio and driving amplitude are exceeded, the gamma distribution emerges robustly and, furthermore, provides a near-*complete* description of surface displacements (over two decades of statistics) with only two parameters that need to be estimated. Spectral analysis indicates that waves within the anomalous region possess an elevated level of high frequencies and exhibit harmonics. These findings, taken together, offer a stringent test for anomalous-wave theories, and may help guide their future development.

While limitations of these idealized experiments certainly should be recognized, many of the basic results may apply more generally to naturally occurring waves. For narrow-band forcing, a normal distribution of surface displacement produces a Rayleigh distribution of wave maxima [44], which has been found to agree generally with ocean observations [2,45]. But circumstances of enhanced nonlinearity, for example, due to variable bathymetry or wind excitation, can produce non-normal statistics with a greater number of extreme waves than expected from the Rayleigh distribution [2,6,28,41]. Interestingly, recent measurements from the Sea of Japan exhibit exponential tails [3], which are comparable to those observed in our experiments and suggest that similar principles may be at work.

We close with a simple calculation for the probability of a "rogue wave" implied by the distributions observed in our experiments. Although conventions vary, let us define a rogue wave as one having a crest exceeding four standard deviations of the surface displacement, i.e., $P(\eta > 4\eta_{\mathrm{std}} \,|\, \eta > 0)$. For a normal distribution, this definition gives a rogue-wave probability of 6.3×10^{-5}, equivalent to most other definitions in the literature [46]. Non-normal distributions, however, may yield different probabilities. For the gamma distribution Eq. (3), in particular, the probability $P(\eta > 4\eta_{\mathrm{std}} \,|\, \eta > 0)$ depends only on the shape parameter, α. The measurements in Fig. 3(b) indicate a typical value of $\alpha = 6.5$ and, in the most extreme case, $\alpha = 4.5$. For these two values, the probability of a rogue wave increases by a factor of 47 and 65, respectively, over a Gaussian distribution, indicating a far greater prevalence of these extreme events.

Acknowledgments. We would like to acknowledge Daniel Kuncicky, Anthony Diaz, and Robert Broedel for valuable assistance in designing, constructing, and operating the experimental apparatus. We would like to thank Andrew J. Majda and Nan Chen for enlightening and inspirational discussions. C.T.B. acknowledges support from the IDEA grant at Florida State University, as well

as from the Geophysical Fluid Dynamics Institute. K.S. acknowledges support from NSF OCE 1231803 and NSF OCE-1536045. M.N.J.M. acknowledges support from the Simons Foundation Collaboration Grants for Mathematicians, award 524259.

[1] Th. A. A. Adcock and P. H. Taylor, The physics of anomalous ('rogue') ocean waves, Rep. Prog. Phys. **77**, 105901 (2014).
[2] K. Dysthe, H. E. Krogstad, and P. Müller, Oceanic rogue waves, Annu. Rev. Fluid Mech. **40**, 287 (2008).
[3] A. Hadjihosseini, J. Peinke, and N. P. Hoffmann, Stochastic analysis of ocean wave states with and without rogue waves, New J. Phys. **16**, 053037 (2014).
[4] C. Kharif and E. Pelinovsky, Physical mechanisms of the rogue wave phenomenon, Eur. J. Mech., B, Fluids **22**, 603 (2003).
[5] P. Müller, C. Garrett, and A. Osborne, Rogue waves, Oceanography **18**, 66 (2005).
[6] L. H. Ying, Z. Zhuang, E. J. Heller, and L. Kaplan, Linear and nonlinear rogue wave statistics in the presence of random currents, Nonlinearity **24**, R67 (2011).
[7] N. Chen and A. J. Majda, Filtering nonlinear turbulent dynamical systems through conditional Gaussian statistics, Mon. Weather Rev. **144**, 4885 (2016).
[8] A. M. S. Macêdo, I. R. R. González, D. S. P. Salazar, and G. L. Vasconcelos, Universality classes of fluctuation dynamics in hierarchical complex systems, Phys. Rev. E **95**, 032315 (2017).
[9] A. Majda and D. Qi, Strategies for reduced-order models for predicting the statistical responses and uncertainty quantification in complex turbulent dynamical systems, SIAM Rev. **60**, 491 (2018).
[10] A. J. Majda, *Introduction to Turbulent Dynamical Systems in Complex Systems* (Springer, New York, 2016).
[11] T. P. Sapsis and A. J. Majda, Blending modified Gaussian closure and non-Gaussian reduced subspace methods for turbulent dynamical systems, J. Nonlinear Sci. **23**, 1039 (2013).
[12] T. P. Sapsis and A. J. Majda, Statistically accurate low-order models for uncertainty quantification in turbulent dynamical systems, Proc. Natl. Acad. Sci. USA **110**, 13705 (2013).
[13] T. P. Sapsis and A. J. Majda, A statistically accurate modified quasilinear Gaussian closure for uncertainty quantification in turbulent dynamical systems, Phys. D (Amsterdam, Neth.) **252**, 34 (2013).
[14] T. B. Benjamin and J. E. Feir, The disintegration of wave trains on deep water part 1. Theory, J. Fluid Mech. **27**, 417 (1967).
[15] A. Chabchoub, N. P. Hoffmann, and N. Akhmediev, Rogue Wave Observation in a Water Wave Tank, Phys. Rev. Lett. **106**, 204502 (2011).
[16] A. Chabchoub, Tracking Breather Dynamics in Irregular Sea State Conditions, Phys. Rev. Lett. **117**, 144103 (2016).
[17] W. Cousins and T. P. Sapsis, Unsteady evolution of localized unidirectional deep-water wave groups, Phys. Rev. E **91**, 063204 (2015).
[18] M. Farazmand and T. P. Sapsis, Reduced-order prediction of rogue waves in two-dimensional deep-water waves, J. Comput. Phys. **340**, 418 (2017).
[19] C. Garrett and J. Gemmrich, Rogue waves, Phys. Today **62**(6), 62 (2009).
[20] M. Onorato, A. R. Osborne, M. Serio, and S. Bertone, Freak Waves in Random Oceanic Sea States, Phys. Rev. Lett. **86**, 5831 (2001).
[21] C. Viotti, D. Dutykh, J. M. Dudley, and F. Dias, Emergence of coherent wave groups in deep-water random sea, Phys. Rev. E **87**, 063001 (2013).
[22] D. R. Solli, C. Ropers, P. Koonath, and B. Jalali, Optical rogue waves, Nature (London) **450**, 1054 (2007).
[23] S. Birkholz, C. Brée, I. Veselić, A. Demircan, and G Steinmeyer, Ocean rogue waves and their phase space dynamics in the limit of a linear interference model, Sci. Rep. **6**, 35207 (2016).
[24] C. Kharif, J.-P. Giovanangeli, J. Touboul, L. Grare, and E. Pelinovsky, Influence of wind on extreme wave events: Experimental and numerical approaches, J. Fluid Mech. **594**, 209 (2008).

[25] A. Toffoli, D. Proment, H. Salman, J. Monbaliu, F. Frascoli, M. Dafilis, E. Stramignoni, R. Forza, M. Manfrin, and M. Onorato, Wind Generated Rogue Waves in An Annular Wave Flume, Phys. Rev. Lett. **118**, 144503 (2017).

[26] M. Onorato, D. Proment, and A. Toffoli, Triggering Rogue Waves in Opposing Currents, Phys. Rev. Lett. **107**, 184502 (2011).

[27] A. Toffoli, T. Waseda, H. Houtani, L. Cavaleri, D. Greaves, and M. Onorato, Rogue waves in opposing currents: An experimental study on deterministic and stochastic wave trains, J. Fluid Mech. **769**, 277 (2015).

[28] E. J. Heller, L. Kaplan, and A. Dahlen, Refraction of a Gaussian seaway, J. Geophys. Res., Oceans **113**, C09023 (2008).

[29] B. S. White and B. Fornberg, On the chance of freak waves at sea, J. Fluid Mech. **355**, 113 (1998).

[30] O. Gramstad, H. Zeng, K. Trulsen, and G. K. Pedersen, Freak waves in weakly nonlinear unidirectional wave trains over a sloping bottom in shallow water, Phys. Fluids **25**, 122103 (2013).

[31] M. Onorato and P. Suret, Twenty years of progresses in oceanic rogue waves: The role played by weakly nonlinear models, Nat. Hazards **84**, 541 (2016).

[32] E. Pelinovsky, T. Talipova, and C. Kharif, Nonlinear-dispersive mechanism of the freak wave formation in shallow water, Phys. D (Amsterdam, Neth.) **147**, 83 (2000).

[33] A. Sergeeva, E. Pelinovsky, and T. Talipova, Nonlinear random wave field in shallow water: Variable Korteweg-de Vries framework, Nat. Hazards **11**, 323 (2011).

[34] K. Trulsen, Rogue waves in the ocean, the role of modulational instability, and abrupt changes of environmental conditions that can provoke non equilibrium wave dynamics, in *The Ocean in Motion* (Springer, New York, 2018), pp. 239–247.

[35] K. Trulsen, H. Zeng, and O. Gramstad, Laboratory evidence of freak waves provoked by non-uniform bathymetry, Phys. Fluids **24**, 097101 (2012).

[36] C. Viotti and F. Dias, Extreme waves induced by strong depth transitions: Fully nonlinear results, Phys. Fluids **26**, 051705 (2014).

[37] R. Höhmann, U. Kuhl, H.-J. Stöckmann, L. Kaplan, and E. J. Heller, Freak Waves in the Linear Regime: A Microwave Study, Phys. Rev. Lett. **104**, 093901 (2010).

[38] C. Tyler Bolles, Water waves over a step: Experiments, simulations, and freak events, Thesis, Florida State University, 2017.

[39] B. J. Landry, M. J. Hancock, C. C. Mei and M. H. García, Wavear: A software tool for calculating parameters for water waves with incident and reflected components, Comput. Geosci. **46**, 38 (2012).

[40] R. Camassa, R. M. McLaughlin, M. N. J. Moore, and K. Yu, Stratified flows with vertical layering of density: Experimental and theoretical study of flow configurations and their stability, J. Fluid Mech. **690**, 571 (2012).

[41] J. Gemmrich and C. Garrett, Unexpected waves, J. Phys. Oceanogr. **38**, 2330 (2008).

[42] A. Toffoli, J. Monbaliu, M. Onorato, A. R. Osborne, A. V. Babanin, and E. Bitner-Gregersen, Second-order theory and setup in surface gravity waves: A comparison with experimental data, J. Phys. Oceanogr. **37**, 2726 (2007).

[43] S. Nazarenko, S. Lukaschuk, S. McLelland, and P. Denissenko, Statistics of surface gravity wave turbulence in the space and time domains, J. Fluid Mech. **642**, 395 (2010).

[44] M. S. Longuet-Higgins, On the statistical distribution of the height of sea waves, J. Mar. Res. **11**, 245 (1952).

[45] O. M. Phillips, D. Gu, and M. Donelan, Expected structure of extreme waves in a Gaussian sea. Part I: Theory and SWADE buoy measurements, J. Phys. Oceanogr. **23**, 992 (1993).

[46] Rogue waves are most commonly defined as the maximum crest-to-trough height exceeding some multiple (often 2 or 2.2) of the significant wave height $H_s = 4\eta_{\text{std}}$. However, we prefer a definition that depends on the surface displacement only, since that quantity can be measured directly in our experiments without the ambiguity and potential statistical bias associated with identifying crests/troughs of randomized wave trains.